Advanced Analysis of Reinforced Concrete

Helmut Hartl
Amt der Burgenländischen Landesregierung, Referat Brückenerhaltung, Österreich

ASTRACT: A 3D (three-dimensional) finite element program has been developed for reinforced and prestressed concrete structures in order to make advanced numerical methods available to engineers. All parameters needed can be taken from the literature (codes, fib-bulletins). Concrete is modeled in terms of plasticity, employing the Ottosen failure criterion. As flow rule serves the Drucker-Prager surface. A robust return is guaranteed by the elasto-visco-plastic approach. A rotating crack model based on the cohesive crack concept is presented for tensile failure. Creep is accounted for by integrating the entire stress history. The program has the capability to account for every single rebar at its exact spatial position by employing embedded 1D elements in order to represent the reinforcement and tendons. The mesh design can be achieved without considering the reinforcement layout. Two methods accounting for slip at the interface between rebar and concrete are presented. The first method introduces a slip degree of freedom and can be addressed as a left hand approach. The second method introduces interface elements supplementary on the constitutive level, after the displacement field is computed. The effect of any kind of prestressing (initial prestressed, post-tensioned, bonded, unbonded) can be modeled easily within both methods. The first case study presents the interface stresses between two concrete layers due to shrinkage and creep, the second case study points the capability of the slip algorithm at a prestressed beam out. In the third example a prestressed and precast concrete girder, which experienced high deformations due to its slenderness and due to shrinkage and creep got reanalyzed.

1 SIGNIFICANCE OF FEM FOR ANALYSING REINFORCED CONCRETE

If the performance of a reinforced or prestressed concrete structure needs to be simulated numerically many nonlinear phenomenon will be encountered over the time and load history, even at low service load levels: shrinkage & creep, cracking and crushing at the concrete end. The reinforcement which is embedded into the concrete behaves nonlinear due to bond slip and may start to yield at high load levels.

Some tools are able to account for such nonlinear effects within a sectional analysis. Though, discontinuous regions cannot be analyzed with such tools and strut and tie models are employed in many situations of practical design. Such models show a possible flux of forces but cannot provide firm information about the serviceability. This is often an issue when an existing structure should be adapted and subjected to higher loads.

A tool for a 3D-analysis of reinforced concrete was developed [Hartl (2002a)]. It allows studying the interaction of several nonlinear effects of reinforced and prestressed concrete structures from the engineering point of view. No solid knowledge of the theoretical framework behind is necessary.

A successful introduction of nonlinear methods into practice can be achieved only, if these methods do require only reasonable time in order to prepare

the input data. This requires that only easily accessible material parameters, which can be understood by an engineer, need to be provided on the one hand. And on the other hand the laborious work of providing the geometric input should be minimized as much as possible.

The advantage of a continuum-mechanics based approach is that nearly no simplification and idealization of the domain is necessary. Such a computer program can account by default for every single rebar at its exact spatial position. Hence, the load-bearing mechanism is computed by the program once the geometry of the domain is provided. The computing expenses are high but acceptable for today's standard computers. Considering the fast development in computer hardware, it is acceptable to increase the computing demand, if the time for preparing the input data can be decreased.

It was a major goal to develop a tool, which gains the capability to investigate soil structure interaction problems as well. In order to be able to combine some of these ideas, it appeared to be necessary that full access to the program code is available and the program should have implemented some features toward these goals. [BEFE (2004)] served as a development platform. The geotechnical part is already covered by the program.

2 MATERIAL MODEL FOR CONCRETE

Concrete behavior is complex and shows a significant scatter. Several models are available for describing the constitutive behavior of concrete but none of them can be regarded as the well accepted concrete model. Sophisticated models may be excellent for special purposes but no better results may be expected in general cases where only limited information about the concrete and the loading history is available.

The employed model is simple in concept. All parameters have a physical meaning and are familiar to an engineer.

2.1 Concrete Crushing

For the sake of simplicity the compressive behavior is assumed linear elastic up to the failure surface [Ottosen (1977)] and perfectly plastic thereafter. This simple approach is able to describe well many engineering situations because the load deformation behavior is indeed nearly linear up to approximately 40% of f_{cm} and even more at high strength concrete. Stresses at service load level will exceed such stress levels rarely. Beyond such stress levels micro-cracks in the concrete matrix induce an anisotropic behavior and the constitutive behavior becomes rather complex. However, the ultimate stress can be described well by a failure surface.

The Ottosen surface is described by four parameters. [Dahl (1992)] proposed for the four parameters an approximation based on experimental data knowing only the compressive strength f_{cm}. The parameters computed according to Dahl can be employed for normal strength concrete and for high strength concrete. The parameters are

$$x = \frac{f_{cm}}{100[\mathrm{MN/m^2}]} \tag{1}$$

$$A = -1.66 \cdot x^2 + 3.49 \cdot x + 0.73 \tag{2}$$

$$B = -0.19 \cdot x^2 + 0.41 \cdot x + 3.13 \tag{3}$$

$$K_1 = 0.46 \cdot x^2 - 0.97 \cdot x + 11.89 \tag{4}$$

$$K_2 = -0.02 \cdot x^2 + 0.04 \cdot x + 0.974 \tag{5}$$

[MC90] gives recommendations for the Ottosen parameters based on the uniaxial compressive and tensile strength of normal strength concrete (f_{ck} < 80MPa).

If this advice is neglected, contradictory results will be obtained as shown in Figure 1. Although the uniaxial compressive strength (f_{cm} = 98MPa) is an input parameter for the failure envelope, it represents a stress state outside the failure envelope (dotted line in Figure 1). This is a clear contradiction. Therefore, the [MC90] recommendations should not be extrapolated for high-strength concrete. But f_{cm} is on the failure envelope if the parameters are computed according to Dahl as shown by the solid line in Figure 1.

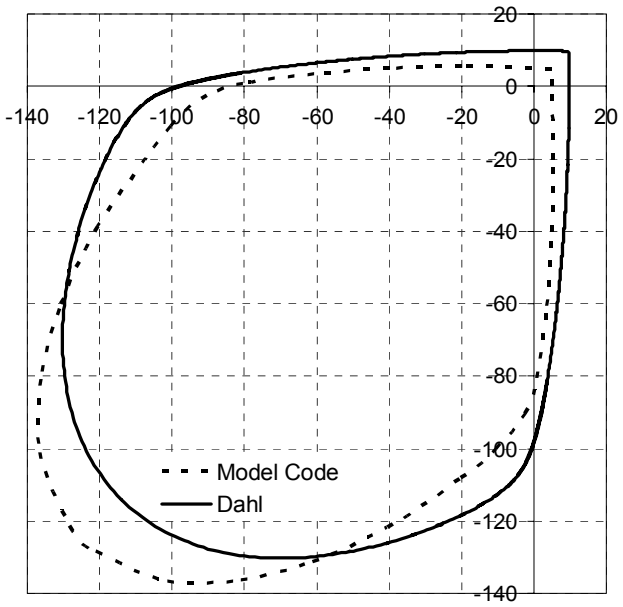

Figure 1 [Ottosen (1977)] envelope for C90/105 (f_{cm} = 98MPa) with parameters according to [Dahl (1992)] vs. [MC90]

A stress state outside the failure surface is not admissible. Plastic strains will develop instead and the stress state will remain on the failure surface. Therefore the computed strain increment must be split into an elastic part which may yield to another stress state on the failure surface and a plastic part which does not produce stresses. Based on experimental observations at ductile materials, it is assumed that the direction of the plastic strain increment is independent on the loading path leading to the failure envelope and on the current loading direction. Thus, a potential function may be employed as flow rule for determination of the plastic strain increment [Melan (1938)]. Although real concrete behavior is much more complex, the Drucker-Prager surface is employed as plastic potential function.

2.1.1 Return algorithm

The elasto-visco-plastic approach is employed as return method [Perzyna (1963), Perzyna (1966)] for its robustness. A stress state outside the yield surface is allowed for $t \neq \infty$ in this method. The stress at time $t + \Delta t$ is

$$\boldsymbol{\sigma}_{t+\Delta t} = \boldsymbol{\sigma}_t - \mathbf{D} \cdot \frac{\Delta t}{\eta} \langle F \rangle \frac{\partial Q}{\partial \boldsymbol{\sigma}} \tag{6}$$

where $\sigma t+\Delta t$ is the stress at time $t+\Delta t$. ***D*** is the elasticity matrix. Q is the plastic potential function, which is in this case the Drucker-Prager cone and F is the [Ottosen (1977)] failure criterion. $\langle F \rangle$ indicates a step function where

$\langle F \rangle = 0$ if $F \leq 0$ (7)

$\langle F \rangle = f_{(F)}$ if $F > 0$ (8)

No material rheology is considered here. Thus, the viscosity parameter η is set to unity and time has no physical meaning. The time reduces to a mere convergence parameter. The plastic strain rate $\partial Q/\partial \boldsymbol{\sigma}$ is multiplied by ***D*** in order to obtain the stress rate. $\Delta t \cdot \langle F \rangle$ can be interpreted as a rate multiplier $\Delta\lambda$ in order to obtain a stress state on the failure surface. This multiplier $\Delta\lambda$, which results in a limiting stress state on the yield surface, is of interest for a fast computation.

$$F_{\left(\boldsymbol{\sigma} - \mathbf{D} \cdot \Delta\lambda \frac{\partial Q}{\partial \boldsymbol{\sigma}}\right)} = 0 \tag{9}$$

An analytical approach towards this issue is shown in [Mang & Hofstetter (2000)]. A numerical approach is shown here. The condition given (9) can be fulfilled numerically by employing an iterative scheme employing the Newton method. The derivative of F_n is approximated by means of the secant connection of two trial points as shown in Figure 2.

$$\boldsymbol{\sigma}_{n+1} = \boldsymbol{\sigma}_n - \mathbf{D} \cdot \frac{F_n}{\frac{F_{n-1} - F_n}{\left\| \boldsymbol{\sigma}_{n-1} - \boldsymbol{\sigma}_n \right\|}} \cdot \frac{\partial Q}{\partial \boldsymbol{\sigma}_0} \tag{10}$$

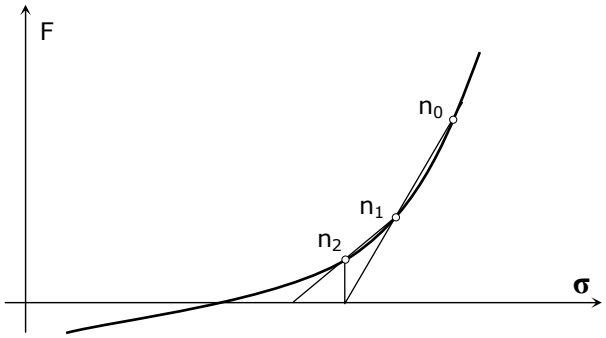

Figure 2 Iterative scheme for obtaining a stress state on the yield surface

The initial trial stress is $\boldsymbol{\sigma}_0 = \boldsymbol{\sigma}_{el}$. Then, a small value is assigned to $\Delta\lambda$ ($= \Delta t \cdot \langle F \rangle$) and $\boldsymbol{\sigma}_1$ is computed by evaluation of (6). For all subsequent steps, (10) applies and a fast convergence is obtained. The final stress is always on the yield surface.

A merit of this elasto-visco-plastic approach is that the derivative of the yield function F is not needed in order to compute $\boldsymbol{\sigma}$. This procedure is appealing when the derivative of the yield function is very involved and costly to compute. Only a smooth plastic potential function is required in order to ensure a robust return.

2.2 Concrete Cracking

Tensile cracking is a dominant source for nonlinear material behavior in reinforced concrete structures. A review of available crack models can be found in [Hofstetter & Mang (1995)].

Cracking is a discrete phenomenon at discrete planes. The first crack plane is initiated perpendicular to the principal axis of any tensile stress higher than f_{ct}. Tensile stresses can be transferred still at any plane perpendicular to the crack plane. Upon subsequent rotation of the principal stress axis, the load transfer mechanism becomes complex: A certain shear stresses can be transferred still over cracks and additional crack planes may develop as well.

At reinforced concrete structures the load transfer mechanism will be controlled dominantly by the reinforcement after cracks have initiated. Hence, a sophisticated model for the shear stress transfer over open cracks seems not to be a primary issue. It is more important that the crack model accounts well for the softening behavior of cracking concrete.

The implemented crack model is formulated within plasticity theory and is based on the smeared crack concept. A crack is assumed to be smeared over the volume represented by the regarding integration point. The model accounts for the introduced anisotropy, unless the user enforces the program to assume an isotropic strength reduction.

In order to account for the anisotropy the plastic strain components (illustrated by the solid Mohr circle in Figure 3) are computed along the principal stress axis and the admissible stress for each principal axis is computed from the regarding plastic strain component. Then, an iterative procedure takes place for the stress update and additional plastic strains may arise along the principal axis. After constitutive relations are satisfied the updated plastic strain components are rotated back to the global coordinate system and stored as shown by the dashed Mohr circle in Figure 3 [Welscher (1993), Hartl (2002a)].

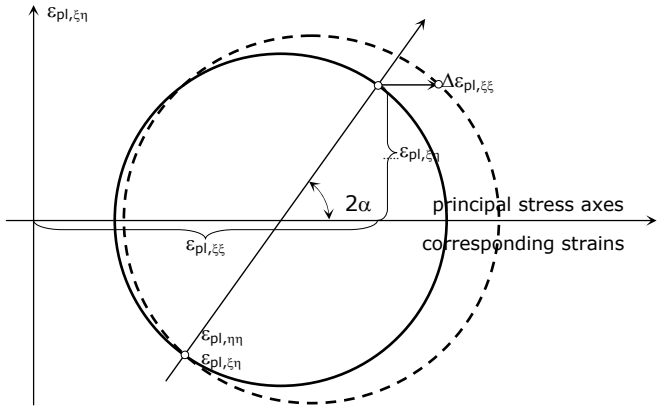

Figure 3 Update of plastic strain

Figure 4 illustrates the behavior at tensile loading. Concrete is assumed to behave linearly elastic up to the tensile limit. The user can provide a tension cut-off factor (1.0 ≥ TCO > 0.0) in order to scale the maximum allowable tensile stress. After a certain amount of tensile flow ε_{yt} has occurred, strain-softening is accounted for in a bilinear fashion in the context of the cohesive crack concept [Hillerborg et al. (1976)]. There the developing crack plane is treated as discrete phenomenon. It is assumed that a certain amount of fracture energy G_F is absorbed by the formation of a unit area of crack surface. The tension softening behavior is now described by a stress elongation diagram, which is controlled by the specific crack energy. This ensures results which are independent of the element size. The parameters for the employed model are given in [MC90]. In the implementation the stress obtained from the model is limited such that: TCO·f_{ctm} ≥ f_{ct} ≥ rTCO·f_{ctm}.

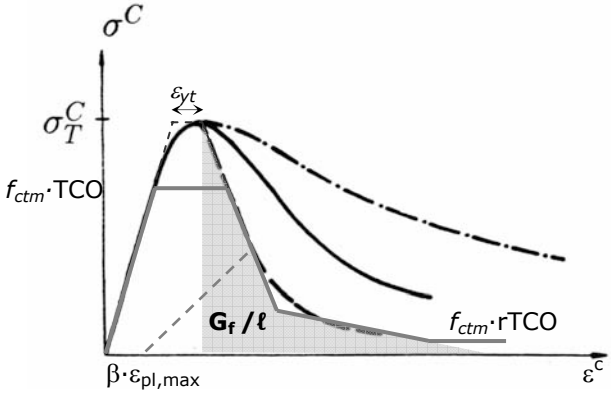

Figure 4 Constitutive behavior of a crack plane at loading and at unloading

At unloading, crack closing is taken into account by reducing the plastic strain increment and a path as illustrated by the dashed line in Figure 4 is followed. The amount of crack closing is controlled

by β. An irreversible crack corresponds to β = 1.0 and a completely recoverable crack corresponds to β = 0.0. According to [Dahlblom & Ottosen (1990)] β= 0.20 may give realistic results.

2.3 Shrinkage & Creep of Concrete

The model implemented into this work is that one of fib bulletin No 1, 1999 [fib1]. This model is able to account for normal strength and for high-performance concrete. Although a model which is based on diffusion theory would be doubtless more appropriate for such a continuum based approach from the physical point of view, the model of fib bulletin No 1 is accepted well in the engineering society and the employed parameters are simple to obtain. On the programming end, the differential equation for diffusion theory need not to be implemented. Since shrinkage is a volumetric process, the 3D shrinkage strain is

$$\boldsymbol{\varepsilon}_{sh}^{T} = \begin{bmatrix} \varepsilon_{sh} & \varepsilon_{sh} & \varepsilon_{sh} & 0 & 0 & 0 \end{bmatrix} \quad (11)$$

The uniaxial shrinkage strain ε_{sh} is dependent on the cement mixture and on the environmental conditions like moisture content of the air and temperature. Creep is additionally dependent on the stress history of the concrete. Procedures which do not require storage of the entire stress history are discussed in [Hofstetter & Mang (1995)]. However, the respective algorithms are not able to account for the general case and are therefore disregarded. The additional computing expenses (especially storage and CPU) for accounting for the entire stress history are no longer genuine computational challenges.

The stress history is approximated on the basis of an implicit midpoint rule as shown in Figure 5 and in (12), [Walter (1988), Hofstetter & Mang (1995)].

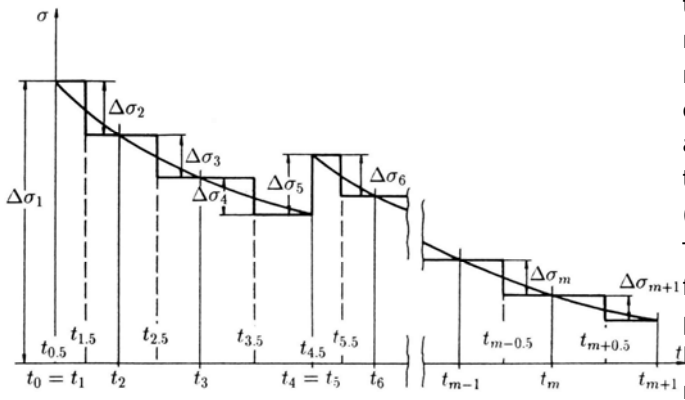

Figure 5 Approximation of the stress history by an implicit integration.

$$\boldsymbol{\varepsilon}_{cc}\left(t_m\right) = \mathbf{A} \cdot \sum_{i=1}^{m} \frac{\varphi\left(t_m, t_{i-1/2}\right)}{E_{ci}} \Delta\boldsymbol{\sigma}\left(t_i, t_{i-1}\right), \quad m \geq 2 \quad (12)$$

No recommendation could be found in literature for the Poisson's ratio of the creep compliance matrix. According to [Bažant & Wittmann (1982)], ν_{cr} may drop almost to zero. If no better value for ν_{cr} is available, ν_{cr} = 0.20 might serve as an acceptable but crude first approximation.

Figure 6 shows the development of creep coefficients for one concrete loaded at different ages.

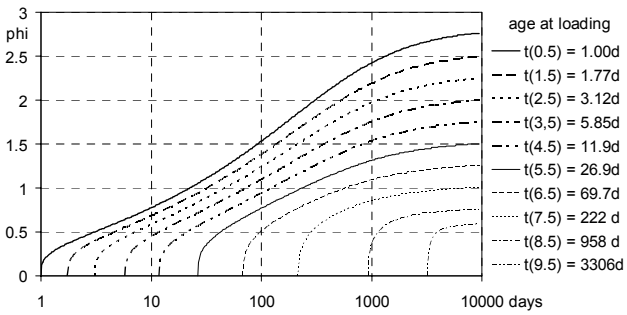

Figure 6 Development of creep coefficients for a generic concrete

At stress levels above a certain limit the relation between stresses and creep strains is no longer linear. For stresses between $0.40 \cdot f_{cm}$ and $0.60 \cdot f_{cm}$, the regarding creep coefficients are modified depending on the current stress level according to [MC90].

3 REPRESENTATION OF THE REINFORCEMENT

The mesh of the parent domain can be prepared independently of the reinforcement layout within the embedded approach. Thus, the mesh can be designed with a high regularity and a variation of the reinforcement or tendon layout does not require a modified mesh for the domain. The reinforcement needs to be provided in global coordinates only. A preprocessing routine detects automatically the intersection of the rebars with the parent element faces as shown by [Hartl (2002a)].

The integration of the stiffness matrix within the finite element framework is straightforward for the parent element. It is the first term of (13). Employing the embedded approach, the reinforcement stiffness is added within the same framework. The employed approach was proposed by [Elwi & Hrudey (1986)] for the 2D case. The

extension to the general 3D case is straightforward, [Cheng (1993)]. The stiffness of the reinforcement is not homogeneous and isotropically distributed over the whole parent element, but available along the reinforcement only. Thus, integration for the reinforcement stiffness has to be performed along the rebar. We have to determine appropriate sample points for the numerical integration (Gauss points) along the reinforcement. The orientation of the reinforcement in this point must be computed, too. The crux in this method is that the integration points of the reinforcement need to be found in local coordinates of the parent elements. This inverse mapping is not straightforward, a Newton root finding algorithm in three dimensions needs to be applied in order to find these integration points for the rebar within the parent element.

$$\mathbf{K}^e = \int_{parent} \mathbf{B}^{eT} \mathbf{D}_c \mathbf{B}^e \cdot dV + \int_{rebar} \mathbf{B}^{eT} \mathbf{T}_{\varepsilon,gl}^T \mathbf{D}_r \mathbf{T}_{\varepsilon,gl} \mathbf{B}^e \cdot dV \quad (13)$$

where **K** is the stiffness matrix, **B** the strain displacement matrix of the parent element, **D** the elasticity matrix of concrete or rebar and **T** the transformation matrix of strains from the global to the local configuration of the rebar.

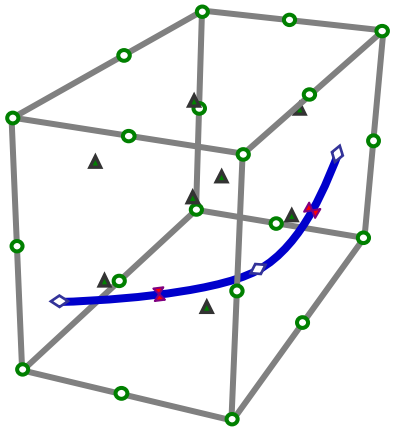

Legend:

- Node of parent element; (DOF, appears in the vector of nodal element displacements)
- Rebar point; (does not appear in the vector of nodal element displacements)
- Integration point for the parent element; (local coordinates of the Gauss points are known)
- Integration point for the rebar; (local coordinates and rebar orientation have to be determined)

Figure 7 Embedded reinforcement bar

Figure 7 shows that the reinforcement is neither restricted to the parent element nodes nor it needs to be parallel to the element boundaries. It can start at any point within the parent element and it can follow a curved path as well.

3.1 Incorporation of bond slip

The displacement field of the parent concrete element applies for the rebar within the embedded approach as well. Thus, perfect bond is obtained. If the slip between the rebar and the concrete should be accounted for, this restriction to perfect bond needs to be relaxed.

One way is to introduce slip degrees of freedom between the parent element and the rebar. Therefore, the finite element program must offer a way to add user-defined elements, since the size of the element stiffness matrix rises for the slip degrees of freedom. Such an approach is shown below. Another way is to introduce the slip supplementary at the material level by relaxing the perfect bond restriction.

3.1.1 Embedded formulation allowing slip

This new developed form of the embedded approach allows the rebar to slip within the parent concrete element. Figure 8 presents a brick element with parabolic shape functions and one embedded rebar. In this special case the size of the element stiffness matrix is increased for the slip degrees of freedom from 60 to 63. The first form of this approach is presented in [Elwi & Hrudey (1986)]. A new easy to follow derivation of this approach is given in [Hartl (2002a)].

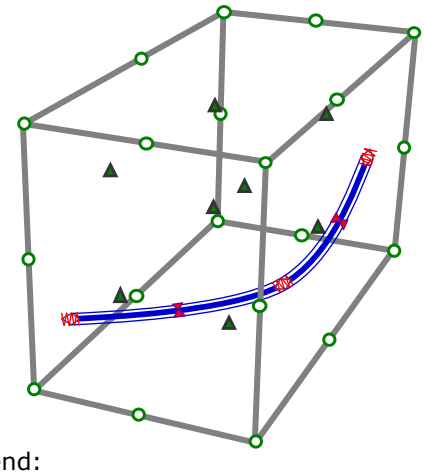

Legend:

- Node of parent element DOF, appears in the vector of nodal element displacements
- Rebar node point DOF, appears in the vector of nodal element displacements
- Integration point for the parent element, local coordinates of the Gauss points are known
- Integration point for the rebar, local coordinates and rebar orientation have to be determined

Figure 8 Embedded reinforcement bar allowing slip

The new introduced DOF is the slip between the concrete and the rebar. The deformation of a rebar point in terms of global coordinates is

$$\mathbf{u}_{r,g} = \begin{bmatrix} \mathbf{N} & 0 & 0 \\ 0 & \mathbf{N} & 0 \\ 0 & 0 & \mathbf{N} \end{bmatrix} \cdot \mathbf{u}^{e}_{parent} + \begin{bmatrix} l_1 \\ m_1 \\ n_1 \end{bmatrix} \cdot u_{slip} \qquad (14)$$

where $\mathbf{N}$ is the shape function matrix for the parent element nodes, $\begin{bmatrix} l_1 & m_1 & n_1 \end{bmatrix}^T$ are the directional cosines for the rebar in the regarding rebar point and **u** is the deformation vector. This equation can be concluded in a form such that the nodal deformations of the element and the slip deformations appear in only one vector. We can rewrite this equation in a form such that

$$\mathbf{u}_{r,g} = \begin{bmatrix} \mathbf{N} & 0 & 0 & l_1 \\ 0 & \mathbf{N} & 0 & m_1 \\ 0 & 0 & \mathbf{N} & n_1 \end{bmatrix} \cdot \mathbf{u}^{e}_{parent+slip} = \mathbf{H} \cdot \mathbf{u}^{e}_{parent+slip} \qquad (15)$$

The internal energy of the brick element with the embedded rebar allowing slip is

$$\Delta\delta W = \int_V \delta\mathbf{u}^{e}_{parent+slip} \cdot \mathbf{H}^T \cdot \mathbf{B}^T_{truss,3D} \cdot E_r \cdot \mathbf{B}_{truss,3D} \cdot \mathbf{H} \cdot \Delta\mathbf{u}^{e}_{parent+slip} \cdot dV \qquad (16)$$

and the stiffness matrix is

$$\mathbf{K} = \mathbf{H}^T \cdot \mathbf{B}^T_{truss,3D} \cdot E_r \cdot \mathbf{B}_{truss,3D} \cdot \mathbf{H} \qquad (17)$$

Within this presented derivation the rebar can slide freely in the duct. An interface element can be introduced now without any difficulties between concrete and rebar. Consequently, any bond-slip situation can be modeled.

3.1.2 Supplementary slip model

Interface elements are introduced supplementary on the material level after the nodal deformations have been computed by the global stiffness matrix. The concept of this so called "supplementary slip model" is shown in Figure 9. The reinforcement is embedded in a classical way without a slip degree of freedom into the parent elements (Figure 9a). Hence, the global analysis computes a deformation of the domain, which assumes perfect bond for the reinforcement. On the material level, this perfect bond situation is relaxed by connecting the reinforcement to the parent elements via continuous interface elements. This is illustrated by a truss analogue (Figure 9b). The truss members are the reinforcement and the supports are represented by the parent elements. The truss elements are connected to the parent elements via bond springs, which are modeled as continuous interface elements. Yet, the strain field of the domain is integrated along the reinforcement path. The deformation of the parent element is applied as support displacement in the truss model. A prestress force can be applied at the truss nodes, [Hartl (2002a)]. The difference in reinforcement forces computed along the truss analogue compared to forces assuming rigid bond, are mapped back as residual nodal forces of the parent element.

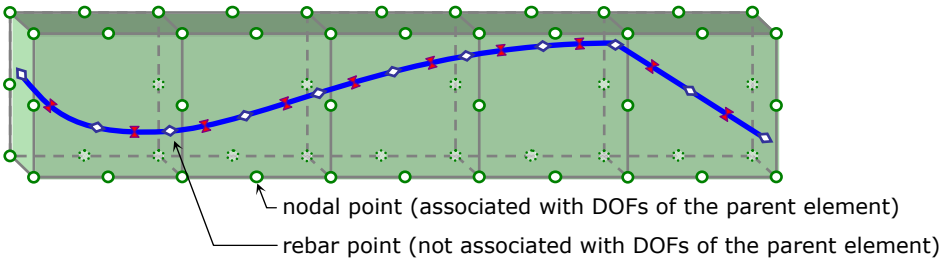

a) Situation in the domain

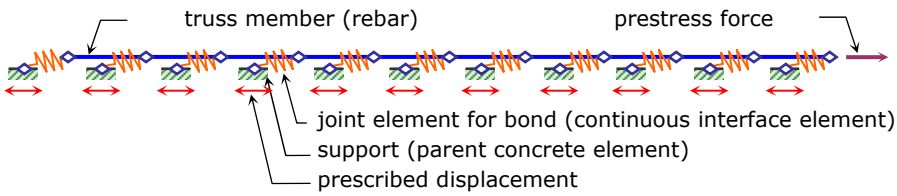

b) Truss model at the material level

Figure 9 Illustration of the supplementary interface model

3.2 Constitutive models for the interface behavior

The constitutive model for an interface needs to be provided as a bond-stress / bond-slip diagram. Slip is the relative displacement between two associated nodes, in this case between a certain node at the rebar and the associated node in the concrete. Two constitutive models are available in the program for the interface between the reinforcement and the parent material. One is the model given in Model Code 90, the other one is the Mohr-Coulomb model.

3.2.1 Mohr-Coulomb interface model

Figure 10 shows the classical Mohr-Coulomb model for frictional situations. The stress acting perpendicular to the interface can be accounted for automatically. Once the peak shear stress is reached, the shear stress is assumed to remain constant with increasing slip. This model is employed for the duct / rebar interface before the duct gets grouted. It can be applied as well for the interface between soil-anchors and the soil or the grout body. Herein, the effect of the overburden stress can be accounted for automatically, as discussed in [Hartl & Pernthaner (2002) Pernthaner (2002)].

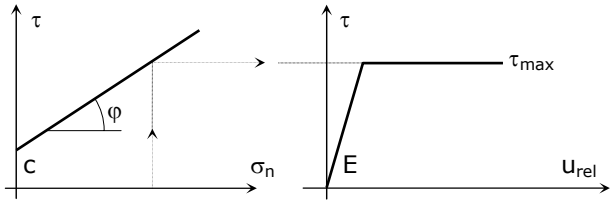

Figure 10 Mohr-Coulomb model (e.g. for the duct / tendon interface)

3.2.2 Model Code 90 interface model

The generic shape of the bond-stress / bond-slip relation given in [MC90] for rebars embedded in concrete is shown in Figure 11. The model has a nonlinear ascending branch (until s_1), an optional yield plateau ($s_1 \div s_2$) at the peak shear stress (τ_{max}), a descending branch ($s_2 \div s_3$) and a residual branch (τ_{res}) from s_3 on. This model is employed in the program for rebars embedded in concrete and for tendons after the duct is grouted. In addition, this model can be adopted for numerous other interface situations as well.

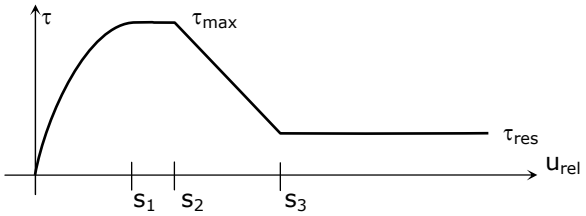

Figure 11 Bond stress - slip diagram acc. to Model Code 90

3.3 Input of a rebar/tendon subjected to slip

The input of a rebar/tendon geometry as shown in Figure 9a is straightforward. The rebar can be provided as a set of polygon points, which are independent of the concrete mesh. If a mid node is provided between two subsequent polygon points, the tendon will follow a parabolic form between these two corner nodes. The program detects the intersection points with the parent element mesh automatically in a preprocessing routine. The interface elements between rebar and concrete are also assigned automatically. Additionally, the cross sectional area, Young's modulus and the yield limit of the rebar need to be provided.

When a prestress force is applied, numerous sequences are encountered during the whole process. The prestress force can be applied in numerous load cases and each time when the hydraulic jack is removed a wedge pull in may occur. Finally, the duct may be grouted in a certain load case. All these described sequences follow generally some typical procedures. For these common procedures, the program supports the user during preparation of the input data for

- bonded tendons
- unbonded tendons
- geotechnical anchors
- initial prestressed wires

4 CASE STUDIES

4.1 Stress at the interface of two concretes

Bridge decks are exposed to traffic and environmental aggression. The concrete cover is removed often during general repair work by high pressure water jetting. In order to enhance the deck for increased traffic loads a new concrete

layer with a certain thickness is often cast on top of the existing deck. The load transfer mechanism and the bearing behavior was investigated experimentally by [Kernbichler (2002a) & (2002b)] and numerically by [Hartl & Sparowitz (2002b)].

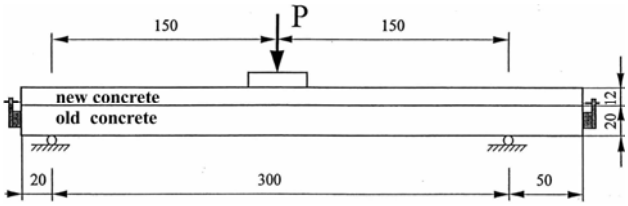

Figure 12 Setup of the experiment, depth of plate 2.50m

The setup of the test is shown in Figure 12. Let us concentrate here on the development of stresses due to shrinkage and creep of these two concretes with different ages. A considerably tensile stress exists at the bottom after the old concrete has experienced creep and shrinkage over 25 years since the reinforcement obstructs the shorting caused by shrinkage as shown in Figure 13a for the right end of the plate. The normal stresses are almost zero at the top of the old concrete since the reinforcement ratio is much lower at the top. The normal stresses in the newly installed concrete are obviously zero at 25 years.

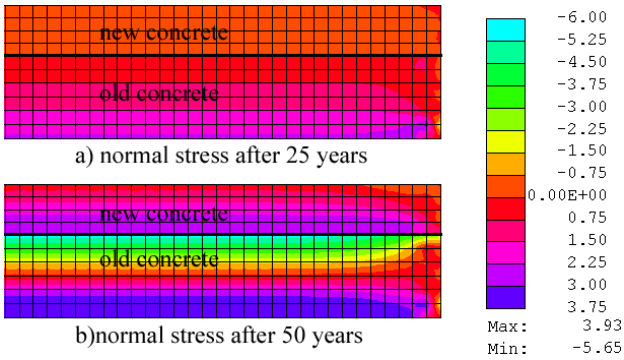

Figure 13 Distribution of normal stresses due to shrinkage and creep.

Figure 13b shows the stress distribution when the new concrete is 25 years old (then the old concrete is 50 years old). The new concrete has high tensile stresses and the old concrete has compressive stresses close to the interface. Shear stresses up to 2MN/m² arise after 50years in the interface between these two concretes without any external load acting as shown in Figure 14 for the right end of the plate. Considering this situation on a Mohr circle, the according principal stress has the same magnitude and is obtained by rotating the axis by 45° since the stress perpendicular to the interface is zero. [Daschner (1976)] observed that concrete develops at a well prepared interface almost the same strength as monolithic concrete. Assuming f_{ctm} ≈ 3MN/m² for the given situation, the shear stress in the interface is utilized at about 2/3 of its ultimate capacity close to the outer end of the plate. And upon loading, the shear stress does not increase in this region as shown in Figure 14b for P = 1000kN.

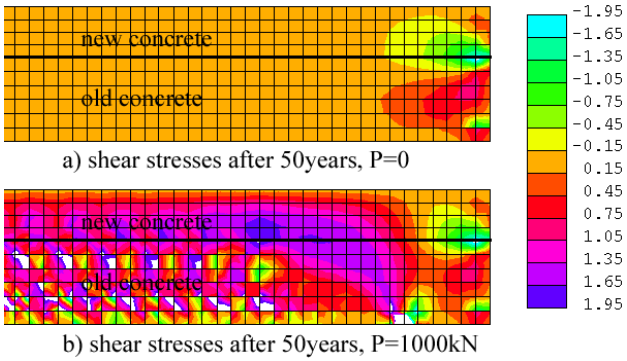

Figure 14 Shear stress after 50 years due to shrinkage and creep

4.2 *Beam with one post tensioned bonded and one post tensioned unbonded tendon*

The example shown in this section is supposed to illustrate the performance of the supplementary slip model. The analyzed beam is shown in Figure 15. The concrete is assumed to behave solely linear elastic and no creep and shrinkage is considered at all. Additional mild reinforcement is not taken into account as well. Hence, only the capability of the supplementary slip model is pointed out here.

The stress resulting from the loads applied are shown in Figure 16. The unbonded tendon 1 gets stressed in load case 1 and the Mohr-Coulomb model interface is employed for the tendon-duct interface. The cohesion is 0.03MN/m^2 and the friction angle is neglected. Tendon 2 is prestressed next. Load case 2 and load case 4 show the stress distribution in the tendons after the wedge-pull-in occurred. The dotted lines show the stress distribution along the rebar calculated by hand utilizing Euler's cable friction theory, where the concrete and the rebar is assumed to be rigid and the interface is assumed to behave rigid-plastic. The numerical solution is smooth since the elastic behavior of the concrete, rebar, and of the interface is taken into account as well. However, both solutions are in good agreement. Tendon 2 gets grouted in load case 5 and the Mohr-Coulomb model is replaced by the Model Code 90 model for

the interface along the tendon. At the end of load case 5 the bonded tendon has started to yield, where the stress increase in the unbonded tendon at this load is comparable small, compare Figure 16. In load case 6 the load is increased such that the unbonded tendon starts to yield as well. The bonded tendon yields in this load case nearly along its entire path. It should be noted again, that no cracking of concrete was taken into account in this special example.

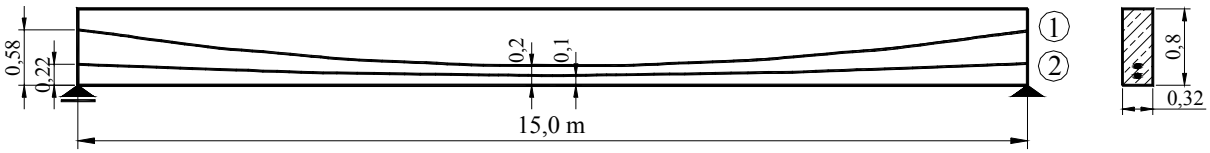

Concrete (linear elastic)	b/h/l = 32 / 80 / 1500 cm		E_c = 32000MN/m^2	ν = 0.20
① unbonded tendon	A_p = 6.00cm^2	f_{yield} = 1385MN/m^2	E_p = 195000MN/m^2	
② bonded tendon	A_p = 6.00cm^2	f_{yield} = 1385MN/m^2	E_p = 195000MN/m^2	

Following load cases are applied to the beam

- Load case 1: Apply a prestress force of 0.785MN to tendon ① + 50% of dead load
- Load case 2: Apply a wedge-pull-in of 1.50mm to the live anchor (left side) of tendon ①
- Load case 3: Apply a prestress force of 0.779MN to tendon ② + 50% of dead load
- Load case 4: Apply a wedge-pull-in of 1.50mm to the live anchor (left side) of tendon ②
- Load case 5: Grout the duct of tendon ② and apply a boundary load q=32.20kN/m
- Load case 6: Apply an additional boundary load q=128.0kN/m

a) Analyzed beam

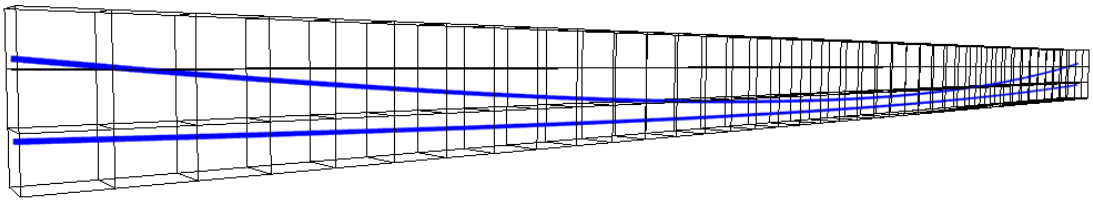

b) Employed mesh for the analysis

Figure 15 Prestressed beam

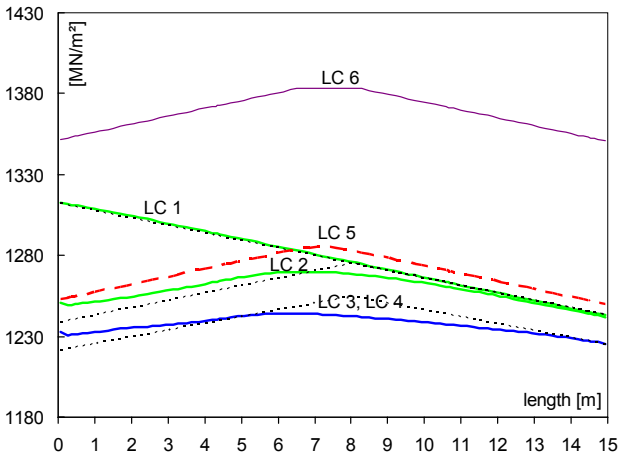

a) Stresses in unbonded tendon ①

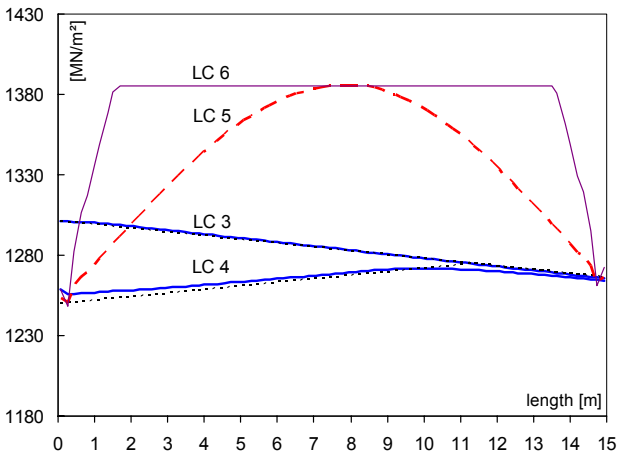

b) Stresses in bonded tendon ②

Figure 16 Tendon stresses

4.3 Roof Girder

The girder shown in Figure 17 is a prestressed roof girder, which has a very high slenderness ratio (h / l ≈ 26). The girder was precast in three parts with concrete C40/50. On the site these three parts got supported by two temporary scaffolds. Then the joints (w = 17.5cm) were cast with concrete C25/30. After the joint concrete had cured for 20 days at winter temperatures the tendons were introduced into the ducts and got prestressed.

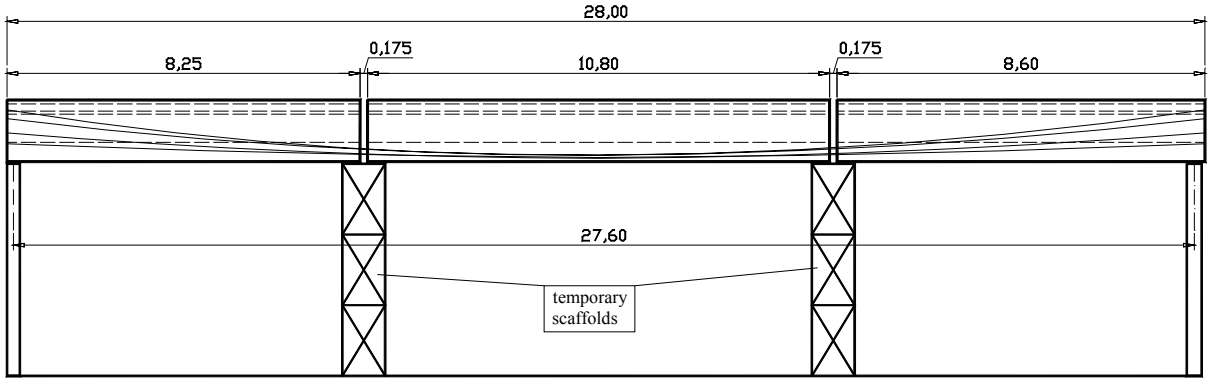

Figure 17 Front view of the shed girder

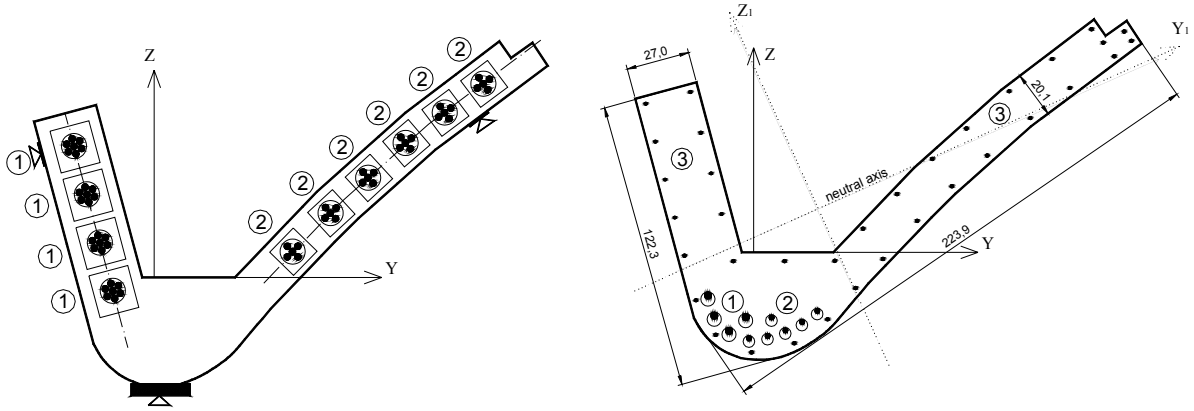

Concrete C40/50 f_{cm} = 48MN/m², f_{ctm} = 3.40MN/m², G_f = 90Nm/m² ν = 0.20 E_c = 32000MN/m²

← bonded tendon (each)	A_p = 6.00cm²	f_{yk} = 1770MN/m²	E_p = 190000MN/m²
↑ bonded tendon (each)	A_p = 4.00cm²	f_{yk} = 1770MN/m²	E_p = 190000MN/m²
→ mild reinforcement (each)	A_p = 0.79cm²	f_{yk} = 500MN/m²	E_p = 200000MN/m²

Figure 18 a) End Cross section of the girder b) Middle cross section of the girder

The construction process described above is accounted for in detail during the analysis. The dead load of the girder is 19kN/m. The permanent load due to the roof covering is 11.37kN/m. The snow load was applied accordingly to the meteorological data for this region (Salzburg/Austria). The highest snow load was 6.46kN/m in winter 1999/00, when the girder was 11 years old. The snow got unloaded in this year after 30 days. Figure 19 shows the deformation over time where the effect of creep and creep-relaxation after unloading the snow can be accounted for in a phenomenological right way, since the entire stress history is stored for the concrete. The stresses in the tendons and in the mild reinforcement can be animated by means of an internet browser at post-processing as shown in Figure 20. For details about the analysis of this girder reference is made to [Handel (2002)].

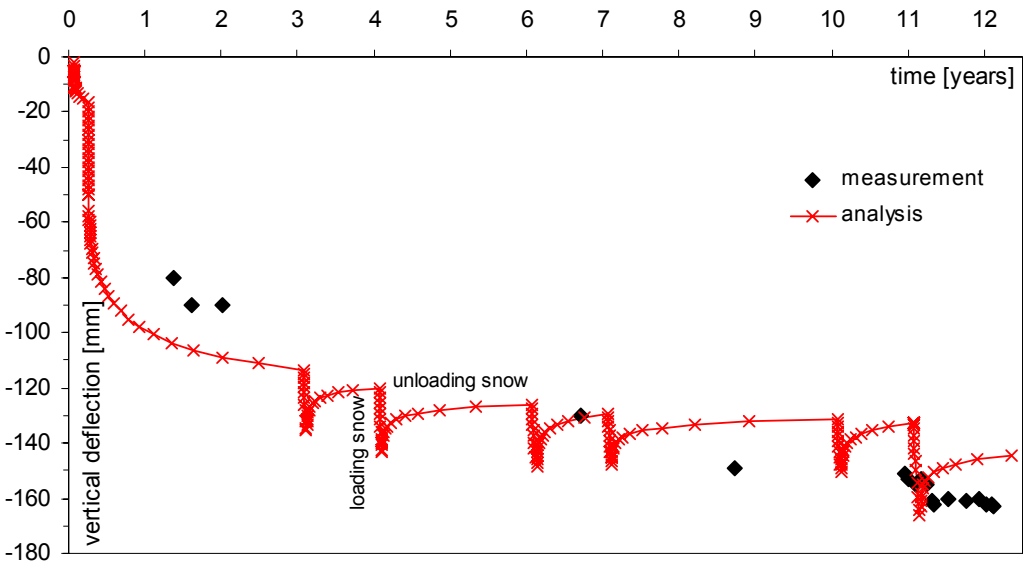

Figure 19 Time - deformation diagram

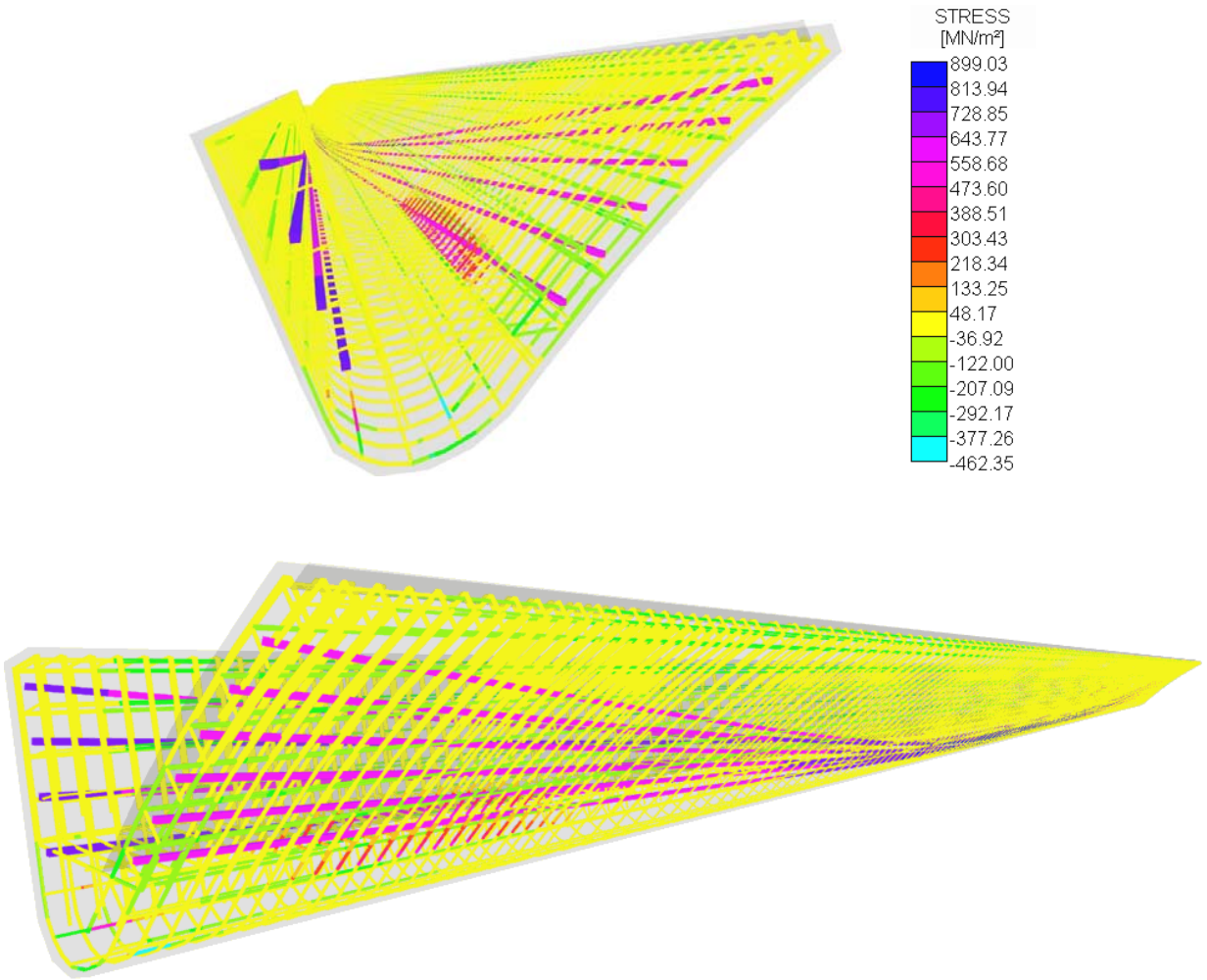

Figure 20 Illustration of stresses in the tendons and in the mild reinforcement after 11 years

5 CONCLUSION & OUTLOOK

The developed program is applied with success in several areas.

- Laboratory tests are reanalyzed with the program for two purposes. On the one hand to get more insight into the structural behavior especially at parameter variations. And, on the other hand to validate the computer program itself.
- For consulting in special cases, especially when the load bearing behavior of existing structures needs to be studied.
- It got used as well in teaching for graduate students. The students got fast familiar with the program and they were able to study the load bearing behavior of a detail as part of their advanced concrete class.

Additional non nonlinear phenomena of reinforced concrete will be implemented into the code as these phenomena appear to be an issue in a case study. However, the presented theory of the described and well tested features can be also implemented into standard FE-codes, like Abaqus or similar ones by means of user routines.

6 REFERENCES

[Bažant, Wittmann (1982)] Bažant Z.P., Wittmann F.H., (eds.), *"Creep and shrinkage in concrete structures"*, John Wiley & Sons, New York, 1982

[BEFE (2004)] Beer G., *"BEFE user's reference and verification manual"*, CSS, Graz, 2004

[Cheng (1993)] Cheng Y.M., Fan Y., "Modeling of reinforcement in concrete and reinforcement confinement coefficient", Finite Elements in Analysis and Design, Elsevier, **13**, 1993, pp. 271-284

[Dahl (1992)] Dahl K.K.B., *"A failure criterion for normal and high strength concrete",* Technical University of Denmark, Lyngby, 1992

[Dahlblom, Ottosen (1990)] Dahlblom O., Ottosen N.S., *"Smeared crack analysis using generalized fictitious crack model",* Journal of Engineering Mechanics, **116**, 1990, pp. 55-76

[Daschner (1986)] Daschner F., *"Versuche zur notwendigen Schubbewehrung zwischen Betonfertigteilen und Ortbeton"*, Deutscher Ausschuß für Stahlbeton, Heft 372, Ernst&Sohn, Berlin, 1986

[Elwi & Hrudey (1989)] Elwi A.E., Hrudey T.M., *"Finite element model for curved embedded reinforcement",* Journal of Engineering Mechanics, **115**, 1989, pp. 740-754

[fib1] fib bulletin No 1, *"Structural concrete"*, vol. 1, International Federation for Structural Concrete (fib), Lausanne, 1999

[Handel (2002)] Handel, Ch., "Traglastberechnung für ein schalenförmiges Sheddach", Diploma Thesis, Institute for Structural Concrete, TU-Graz, Graz, 2002 (in German)

[Hartl & Pernthaner (2002)] Hartl H., Pernthaner M., *"Soil anchors modeled by an embedded formulation allowing slip"*, Proceedings of the second international conference on soil structure interaction in urban civil engineering, COST Action C7, Institute for Geotechnical Engineering, Swiss Federal Institute of Technology Zurich, Zurich, 2002, pp. 123-128

[Hartl & Sparowitz (2002)] Hartl H., Sparowitz L., *"A 10 Tauernautobahn, Brücken-verstärkung F8/F8a und F9, Numerische Untersuchung des Tragverhaltens nachträglich ergänzter Stahlbeton-platten",* Institute for Structural Concrete, TU-Graz, Graz, 2002

[Hartl (2002)] Hartl H. *"Development of a Continuum-Mechanics-Based Tool for 3D Finite Element Analysis of Reinforced Concrete Structures and Application to Problems of Soil-Structure Interaction"*, Doctoral Thesis, Graz University of Technology, Austria, 2002

[Hillerborg et al. (1976)] Hillerborg A., Modeer M., Peterson P.E., *"Analysis of crack formation and crack growth in concrete by means of fracture mechanics and finite elements"*, Cement and Concrete Research, **6**, 1976, pp. 773-782

[Hofstetter, Mang (1995)] Hofstetter G., Mang H.A., *"Computational mechanics of reinforced concrete structures",* Vieweg, Braunschweig, 1995

[Kernbichler (2002a)] Kernbichler K., *"A10*

Tauernautobahn / Brückenverstärkung F8 / F8A und F9: Bericht über experimentelle Untersuchung des Tragverhaltens nachträglich ergänzter Stahlbetonplatten", Konstruktive Versuchsanstalt, Graz University of Technology, Graz, 2002

[Kernbichler (2002b)] Kernbichler K., *"A10 Tauernautobahn / Brückenverstärkung F8 / F8A und F9: Bericht über ergänzende experimentelle Untersuchung des Tragverhaltens nachträglich ergänzter Stahlbetonplatten*", Konstruktive Versuchsanstalt, Graz University of Technology, Graz, 2002

[Mang & Hofstetter (2000)] Mang H., Hofstetter G., *"Festigkeitslehre"*, Springer, Wien, 2000

[MC90 (1993)] CEB-FIP Comitè Euro-International du Bèton, "CEB-FIP Model Code 1990", London, Thomas Telford, 1993

[Melan (1938)] Melan E., *"Zur Plastizität des räumlichen Kontinuums"*, Ingenieur-Archiv, **9**, 1938, pp. 116-126

[Ottosen (1977)] Ottosen N.S., *"A failure criterion for concrete",* Journal of the Engineering Mechanics Division, **103**, 1977, pp. 527-535

[Pernthaner (2002)] Pernthaner M., *"Interaktion von Schlitzwand und Baugrund unter Berücksichtigung der Nichtlinearität der Betonkonstruktionen"*, Diploma Thesis, Institute for Structural Concrete, TU-Graz, Graz, 2002 (in German)

[Perzyna (1963)] Perzyna P. *"The constitutive equations for rate sensitive plastic materials"*, Quarterly of Applied Mathematics, **20**, 1963, pp. 321-332

[Perzyna (1966)] Perzyna P., *"Fundamental problems in viscoplasticity"*, Advances in Applied Mechanics, **9**, 1966, pp. 243-377

[Walter (1988)] Walter H., *"Finite Elemente Berechnungen von Flächentragwerken aus Stahl- und Spannbeton unter Berücksichtigung von Langzeitverformungen und Zustand II"*, Doctoral Thesis, TU-Vienna, Vienna, 1988

[Welscher (1993)] Welscher S., *"Implementierung und Anwendung eines elasto-plastischen Werkstoffmodells für Beton"*, Master Thesis, Institute for Strength of Materials, TU-Vienna, Vienna, 1993